

# VLTI/AMBER and VLTI/MIDI spectro-interferometric observations of the B[e] supergiant CPD–57° 2874\*

## Size and geometry of the circumstellar envelope in the near- and mid-IR

A. Domiciano de Souza<sup>1</sup>, T. Driebe<sup>1</sup>, O. Chesneau<sup>2</sup>, K.-H. Hofmann<sup>1</sup>, S. Kraus<sup>1</sup>,  
A. S. Miroshnichenko<sup>1,3</sup>, K. Ohnaka<sup>1</sup>, R. G. Petrov<sup>4</sup>, Th. Preibisch<sup>1</sup>, P. Stee<sup>2</sup>,  
G. Weigelt<sup>1</sup>, F. Lisi<sup>5</sup>, F. Malbet<sup>6</sup>, and A. Richichi<sup>7</sup>

<sup>1</sup> Max-Planck-Institut für Radioastronomie, Auf dem Hügel 69, 53121 Bonn, Germany

<sup>2</sup> Observatoire de la Côte d’Azur, Gemini, CNRS UMR 6203, Avenue Copernic, 06130 Grasse, France

<sup>3</sup> Dept. of Physics and Astronomy, P.O. Box 26170, University of North Carolina at Greensboro, Greensboro, NC 27402–6170, USA

<sup>4</sup> Laboratoire Universitaire d’Astrophysique de Nice (LUAN), CNRS UMR 6525, UNSA, Parc Valrose, 06108 Nice, France

<sup>5</sup> INAF-Osservatorio Astrofisico di Arcetri, Istituto Nazionale di Astrofisica, Largo E. Fermi 5, I-50125 Firenze, Italy

<sup>6</sup> Laboratoire d’Astrophysique de Grenoble, UMR 5571 Université Joseph Fourier/CNRS, BP 53, 38041 Grenoble Cedex 9, France

<sup>7</sup> European Southern Observatory, Karl Schwarzschild Strasse 2, 85748 Garching, Germany

Received < date > / Accepted < date >

**Abstract.** We present the first high spatial and spectral observations of the circumstellar envelope (CSE) of a B[e] supergiant (CPD–57° 2874), performed with the Very Large Telescope Interferometer (VLTI). Spectra, visibilities, and closure phase, were obtained using the beam-combiner instruments AMBER (near-IR interferometry with three 8.3 m Unit Telescopes or UTs) and MIDI (mid-IR interferometry with two UTs). The interferometric observations of the CSE are well fitted by an elliptical Gaussian model with FWHM diameters varying linearly with wavelength. Typical diameters measured are  $\simeq 1.8 \times 3.4$  mas or  $\simeq 4.5 \times 8.5$  AU (adopting a distance of 2.5 kpc) at  $2.2 \mu\text{m}$ , and  $\simeq 12 \times 15$  mas or  $\simeq 30 \times 38$  AU at  $12 \mu\text{m}$ . The size of the region emitting the Br $\gamma$  flux is  $\simeq 2.8 \times 5.2$  mas or  $\simeq 7.0 \times 13.0$  AU. The major-axis position angle of the elongated CSE in the mid-IR ( $\simeq 144^\circ$ ) agrees well with previous polarimetric data, hinting that the hot-dust emission originates in a disk-like structure. In addition to the interferometric observations we also present new optical ( $UBVR_cI_c$ ) and near-IR ( $JHKL$ ) broadband photometric observations of CPD–57° 2874. Our spectro-interferometric VLTI observations and data analysis support the non-spherical CSE paradigm for B[e] supergiants.

**Key words.** Techniques: high angular resolution – Techniques: interferometric – Infrared: stars – Stars: early-type – Stars: emission-line, Be – Stars: mass-loss – Stars: individual: CPD–57° 2874

## 1. Introduction

Supergiant B[e] (sgB[e]) stars are luminous ( $\log L/L_\odot > 4.0$ ) post-main sequence objects showing the B[e] phenomenon (Lamers et al. 1998): (1) strong Balmer emission lines, (2) low-excitation emission lines of Fe II, [Fe II], and [O I], and (3) strong near/mid-infrared (IR) excess due to hot circumstellar dust. Spectroscopic and polarimetric

observations suggest that sgB[e] stars have non-spherical circumstellar envelopes (CSE; e.g., Zickgraf et al. 1985; Magalhães 1992). Zickgraf et al. (1985) proposed an empirical model of the sgB[e] CSE that consists of a hot and fast line-driven wind in the polar regions, and a slow, much cooler and denser wind (by a factor of  $10^2 - 10^3$ ) in the equatorial region, where dust could be formed. Rapid rotation of the central star seems to play a key role in the origin of the CSE, but a complete explanation of its formation mechanism is still unknown.

To investigate these crucial questions concerning the origin, geometry, and physical structure of the sgB[e] CSE,

Send offprint requests to: A. Domiciano de Souza,  
e-mail: Armando.Domiciano@unice.fr

\* Based on observations obtained with the VLTI of the European Southern Observatory (ESO), Chile

it is necessary to combine several observing techniques. In particular, the high spatial resolution provided by optical/IR long-baseline interferometry allows us to directly probe the vicinity of these complex objects. In this paper we present the first direct multi-wavelength measurements of the close environment of a Galactic sgB[e] star, namely CPD–57° 2874 (WRAY 15-535), using the VLTI with its instruments AMBER and MIDI.

CPD–57° 2874 is a poorly-studied object, for which McGregor et al. (1988) suggested a distance of  $d = 2.5$  kpc, assuming that it belongs to the Carina OB association. A high reddening and the presence of CO emission bands at  $2.3 - 2.4 \mu\text{m}$  makes it compatible with the sgB[e] class. Zickgraf (2003) obtained high-resolution optical spectra exhibiting double-peaked emission lines that are suggestive of a flattened CSE geometry, typical for sgB[e] stars. However, the physical parameters of neither the star nor its CSE have been studied in detail yet.

## 2. Interferometric observations and data reduction

### 2.1. VLTI/AMBER (*near-IR*)

CPD–57° 2874 was observed on 2005 February 25 using the VLTI/AMBER instrument (e.g., Petrov et al. 2003) to combine the light from the 8.3 m Unit Telescopes UT2, UT3, and UT4. With an exposure time of 85 ms, 3000 spectrally dispersed interferograms (frames) were recorded on the target and calibrator (HD 90393). This allowed us to obtain spectra as well as wavelength-dependent visibilities and a closure phase in the  $K$  band with a spectral resolution of  $R = 1500$  between  $2.09$  and  $2.24 \mu\text{m}$  (including the  $\text{Br}\gamma$  line).

Data reduction was performed with the *amdlib* software (Millour et al. 2004; Malbet et al. 2005). We checked the consistency of our results by selecting a fixed percentage of frames from the target and calibrator data sets, based on the fringe contrast signal-to-noise ratio. By keeping 50%, 30%, and 10% of the frames with the best SNR, we found that the derived quantities were stable (differences  $\lesssim 4\%$ ). Moreover, we also found good agreement between the results from the *amdlib* software and our own software based on a power spectrum analysis.

### 2.2. VLTI/MIDI (*mid-IR*)

We also observed CPD–57° 2874 with the VLTI/MIDI instrument (Leinert et al. 2004) on 2004 December 28 and 30. The  $N$ -band spectrum as well as spectrally dispersed fringes have been recorded between  $7.9$  and  $13.5 \mu\text{m}$  with a spectral resolution of  $R = 30$ , allowing us to study the wavelength dependence of the apparent size of CPD–57° 2874 in the mid-IR. In total, 4 data sets have been obtained using the UT2-UT3-47m and UT3-UT4-62m baselines. Several calibrator stars were observed: HD 37160, HD 50778, HD 94510, and HD 107446.

Data reduction was performed with the MIA (Leinert et al. 2004) and EWS (Jaffe 2004) packages. While MIA

**Table 1.** AMBER and MIDI observation log for CPD–57° 2874.

AMBER ( $2.09 \leq \lambda \leq 2.24 \mu\text{m}$ )				
3 Unit Telescopes				
night	$t_{\text{obs}}$ (UTC)	UT baseline	$B_p$ (m)	PA (°)
2005-02-26	03:41:21	UT2-UT3	43.5	37.8
		UT3-UT4	59.8	98.8
		UT2-UT4	89.4	73.6
MIDI ( $7.9 \leq \lambda \leq 13.5 \mu\text{m}$ )				
2 Unit Telescopes				
night	$t_{\text{obs}}$ (UTC)	UT baseline	$B_p$ (m)	PA (°)
2004-12-29	05:52:12	UT2-UT3	45.2	18.5
		UT2-UT3	43.9	35.1
2004-12-31	06:04:03	UT3-UT4	54.8	79.6
		UT3-UT4	60.9	104.8

follows the classical power spectrum analysis, in the EWS software the fringes are coherently added after correction for the instrumental and atmospheric delay in each scan. The visibilities derived with both softwares agree within the uncertainties of  $\simeq 10\%$ .

The logs of the AMBER and MIDI observations are given in Table 1, while Fig. 1 shows the projected baseline lengths  $B_p$  and corresponding position angles PA used. In Table 2 we list the uniform disc diameters  $\theta_{\text{UD}}$  and observation log for the calibrators. Calibrated visibilities from both AMBER and MIDI observations were obtained using the known uniform disk diameters of the calibrator stars (Richichi et al. 2005), which were observed in the same nights as CPD–57° 2874.

## 3. Photometric observations

In addition to the VLTI data we also present here new broadband photometric observations of CPD–57° 2874. Optical ( $UBVR_cI_c$ ) and near-IR ( $JHKL$ ) photometric observations were obtained quasi-simultaneously on 1997 July 10 at the South-African Astronomical Observatory (SAAO). Additional near-IR observations were obtained on 1997 June 15 and December 28. The 0.75-meter telescope with a single-element InSb photometer (Carter 1990) was used in the near-IR, while the 0.5-meter telescope with a GaAs photometer (Menziés et al. 1991) was used in the optical region.

The data are presented in Table 3. The errors in the tabulated magnitudes and colors are not greater than 0.02 mag. A number of standard stars were observed during the same nights for calibration.

Our photometric results are very close to a few published observations of the star. Drilling (1991) obtained 3  $UBV$  observations in 1972–1976 ( $V=10.20$ ;  $B - V=1.66$ ,  $U - B=0.41$  mag; the colon indicates either a variabil-

**Table 3.** Photometry of CPD–57° 2874 obtained at SAAO.

JD 2450000+	$V$	$U - B$	$B - V$	$V - R_c$	$V - I_c$	$J$	$H$	$K$	$L$
615.29						5.76	4.87	4.02	2.73
640.21						5.80	4.88	4.03	2.74
640.23	10.08	0.30	1.65	1.23	2.39				
811.57						5.74	4.86	4.02	2.73

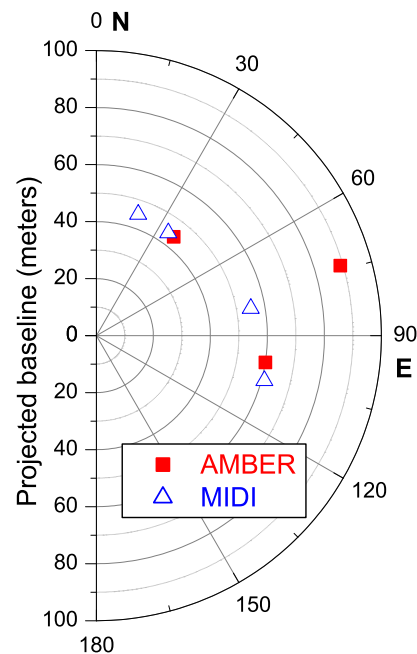
**Table 2.** Uniform disc diameters and observation log for the calibrators.

AMBER ( $2.09 \leq \lambda \leq 2.24 \mu\text{m}$ ) 3 Unit Telescopes			
Calibrator HD number	$\theta_{\text{UD}}$ (mas)	night	$t_{\text{obs}}$ (UTC)
90393	$0.77 \pm 0.01$	2005-02-26	04:38:04
MIDI ( $7.9 \leq \lambda \leq 13.5 \mu\text{m}$ ) 2 Unit Telescopes			
Calibrator HD number	$\theta_{\text{UD}}$ (mas)	night	$t_{\text{obs}}$ (UTC)
37160	$2.08 \pm 0.20$	2004-12-29	04:12:26 05:29:32
50778	$3.95 \pm 0.22$	2004-12-29 2004-12-31	06:13:08 02:15:59 03:04:33
94510	$2.16 \pm 0.11$	2004-12-29 2004-12-31	07:47:21 06:31:19 07:41:22
107446	$4.54 \pm 0.23$	2004-12-31	07:19:17

ity suspicion or an uncertainty of over 0.08 mag), and McGregor et al. (1988) obtained near-IR observations on 1983 May 15 ( $J = 5.77$ ,  $H = 4.99$ ,  $K = 4.02$  mag). The 2MASS data obtained on 2000 January 18 (Cutri et al. 2003) are very similar ( $J = 5.76$ ,  $H = 4.96$ ,  $K = 4.3 \pm 0.3$  mag). However, the near-IR fluxes from Swings & Allen (1972) are very different:  $K = 5.44$ ,  $H - K = 0.33$ ,  $K - L \sim 0.7$  mag. Also, Wackerling (1970) quotes  $m_{\text{vis}} = 8.6$  mag and  $m_{\text{pg}} = 10.2$  mag<sup>1</sup>. This information is not sufficient to conclude whether any brightness changes occurred in the early 1970s, but it indicates that the optical and near-IR fluxes have been stable for the last 30 years.

Analysis of the available photometric and spectroscopic data for the object and its neighborhood allows us to put some constraints on the basic parameters of the underlying star and the distance toward it, an issue that has never been carefully addressed. The observed set of emission lines in the optical region (H I, He I, Fe II; Zickgraf 2003, McGregor et al. 1988, Carlson & Henize

<sup>1</sup>  $m_{\text{pg}}$  means photographic magnitude, which is usually considered a rough analog of a B-band photometry.

**Fig. 1.** Projected baselines and corresponding position angles for the AMBER and MIDI observations of CPD–57° 2874 (see also Table 1).

1979, and others) suggests that the star has an early B spectral type, which in combination with the large optical colour-indices implies a high reddening (see Table 3). However, the presence of a significant amount of gas and dust in the object’s CSE makes uncertain whether the entire reddening is interstellar. On the other hand, this is most likely the case, because the observed  $U - B$  and  $B - V$  colour-indices are in agreement with the interstellar reddening slope for the stars in the object’s direction ( $E(U - B)/E(B - V) = 0.74 \pm 0.06$ ). If we ignore the possible impact of the CSE gas on the object’s SED, then dereddening with the above colour-index ratio gives  $E(B - V) = 1.85$  mag and the spectral type  $B1 \pm 1$  (also in agreement with the spectral line content). Moreover, strong diffuse interstellar bands (at  $\lambda 5780 \text{ \AA}$  and  $\lambda 5797 \text{ \AA}$ ) are present in the spectrum, and their strengths are consistent with the  $E(B - V)$  (Herbig 1993).

Adopting the typical galactic total-to-selective interstellar extinction ratio  $A_V/E(B - V) = 3.1$  for early-type stars, we get  $A_V = 5.8$  mag and the intrinsic visual bright-

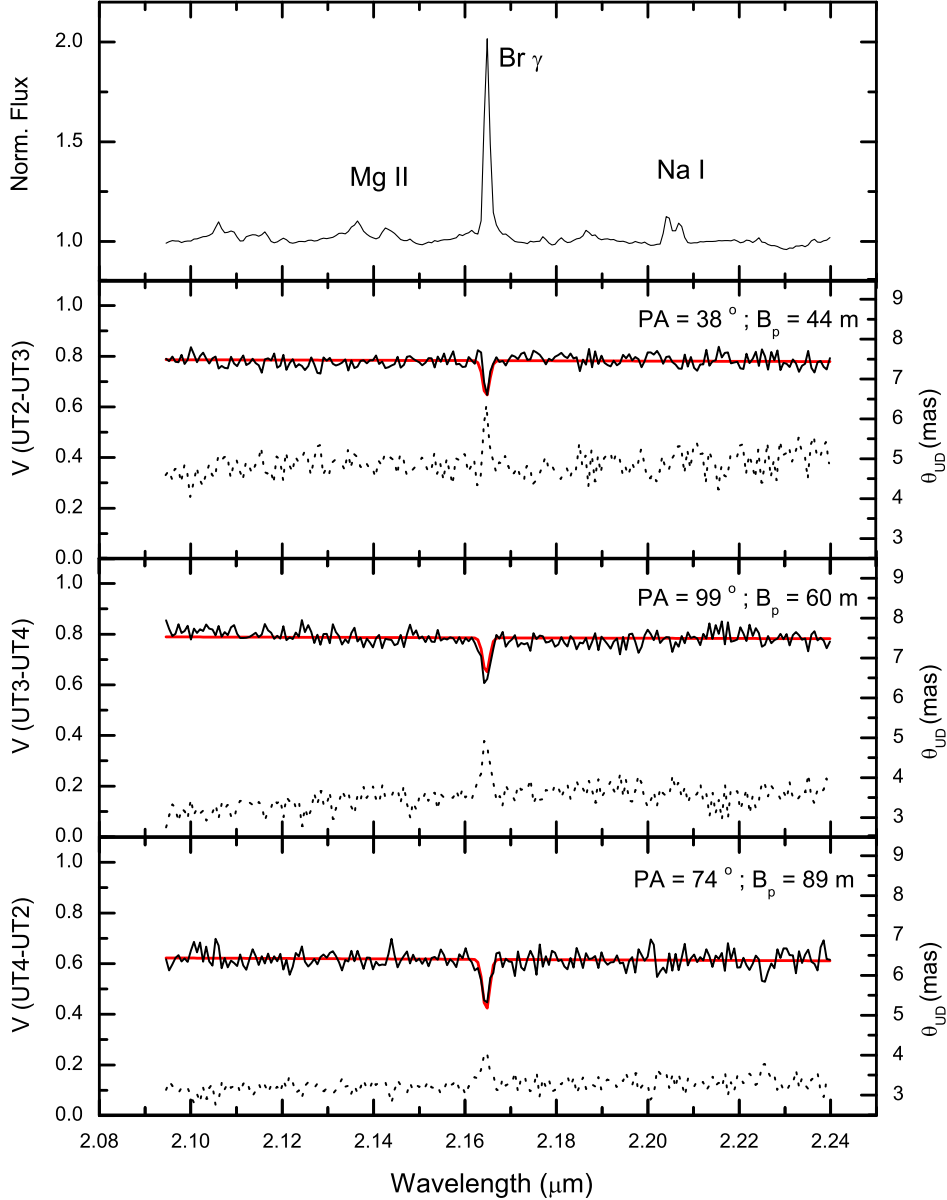


**Fig. 2.** VLTI/AMBER observations of CPD-57° 2874 obtained around Br $\gamma$  with spectral resolution  $R = 1500$ . The normalized flux is shown in the top panel and the visibilities  $V$  for each baseline (30% best frames) are given in the other panels (the corresponding projected baselines  $B_p$  and position angles PA are indicated). The errors in  $V$  are  $\simeq \pm 5\%$ . The dotted lines are the uniform disk angular diameters  $\theta_{UD}$  (to be read from the scales on the right axis), computed from  $V$  at each  $\lambda$  as a zero-order size estimate. The visibilities obtained from the elliptical Gaussian model fit the observations quite well (smooth solid lines; Eqs. 1 and 2, and Table 4). In contrast to the Br $\gamma$  line, the Mg II and Na I lines do not show any clear signature on the visibilities.

ness  $V_0 = 4.3$  mag. Such a brightness, in combination with the high reddening, implies a high stellar luminosity. Since a few nearby A-type stars of 9–10 mag have negligible reddenings, there is almost no interstellar extinction in the object’s direction closer than  $\sim 1$  kpc. Even at such a distance, CPD-57°2874 would be a supergiant ( $\log L/L_\odot \sim 5$ ). An upper limit for the distance ( $\sim 3$  kpc) is set by the Humphreys-Davidson luminosity limit ( $\log L/L_\odot \sim 6$ , Humphreys & Davidson 1979). Thus, the most probable range for the object’s distance is  $2.5 \pm 0.5$  kpc. It is difficult to constrain it bet-

ter due to the unknown contribution of the CSE gas to the star’s brightness, possible anomalous extinction by the CSE dust, and the absence of high-resolution spectroscopic data that show photospheric lines and allow us to measure their radial velocities. The distance determination using galactic kinematic models and available radial velocities of the emission lines is uncertain, because the line profiles are double-peaked. The interstellar extinction law in the object’s direction indicates a patchy structure of dust in the line of sight and hampers further improvement of the above distance estimate.

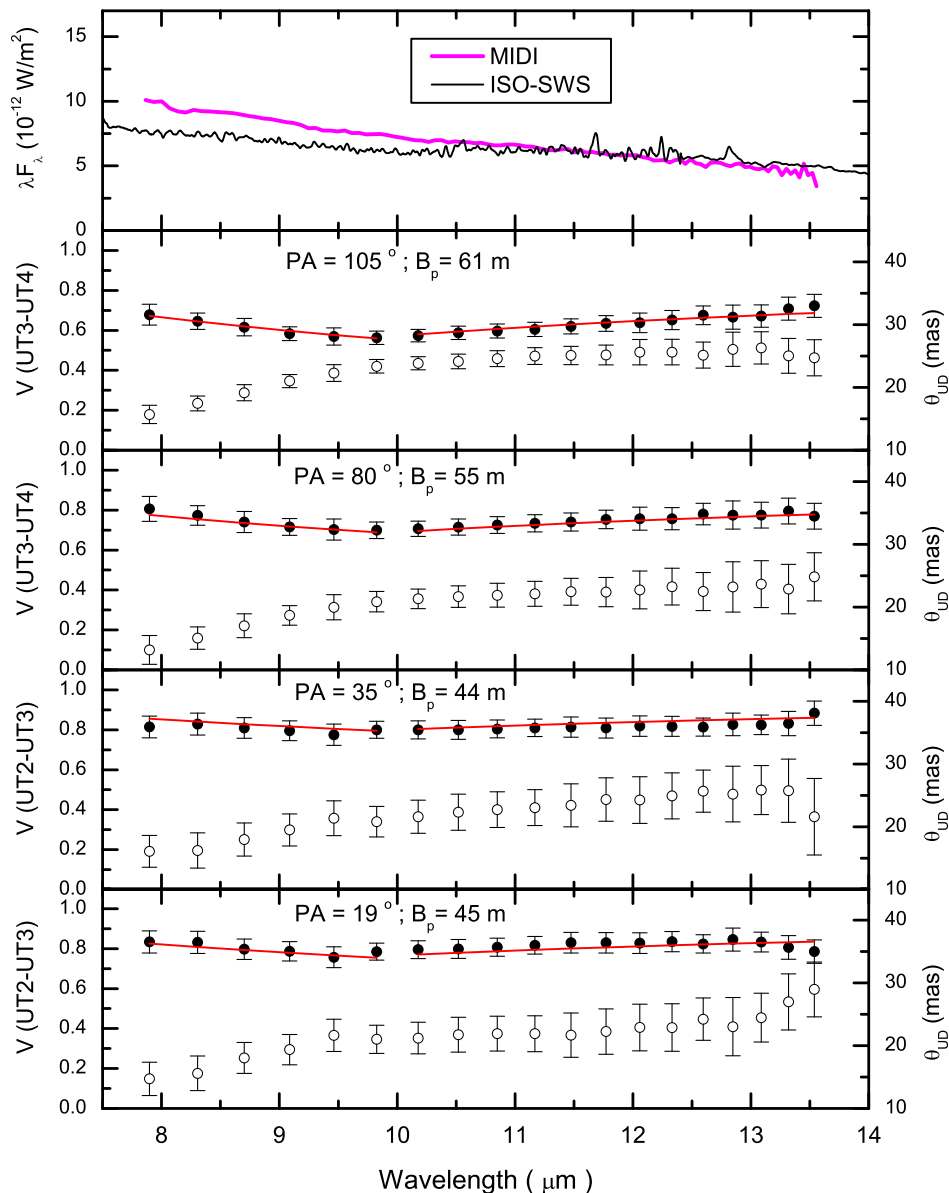


**Fig. 3.** VLTI/MIDI observations of CPD-57° 2874 obtained in the mid-IR with spectral resolution  $R = 30$ . This figure is organized as Fig. 2, but here  $V$  and  $\theta_{\text{UD}}$  are shown as filled and open circles, respectively. The MIDI and ISO-SWS (Sloan et al. 2003) spectra (top panel) do not show any clear evidence of a silicate feature around  $10 \mu\text{m}$ . The MIDI visibilities are well fitted with an elliptical Gaussian model (solid lines; Eqs. 1 and 2, and Table 4).

Summarizing the above discussion, we adopt the following parameters for CPD-57°2874:  $d = 2.5 \pm 0.5$  kpc,  $T_{\text{eff}} = 20000 \pm 3000$  K,  $A_V = 5.8$  mag. They lead to an estimate for the star’s radius of  $R_\star = 60 \pm 15 R_\odot$ .

#### 4. Results

Figures 2 and 3 show the spectra and visibilities obtained with AMBER and MIDI, respectively. CPD-57° 2874 is resolved in both spectral regions at all projected baselines  $B_p$  and position angles PA. As a zero-order size estimate these figures also show the uniform disk angular diameters  $\theta_{\text{UD}}$  obtained from the visibilities at each spectral channel. The size of the region emitting the Br $\gamma$  line is larger than

the region emitting the near-IR continuum. Moreover, the mid-IR sizes are much larger than those in the near-IR.

The AMBER observations also reveal a zero closure phase (Fig. 4) at all wavelengths (within the noise level of a few degrees). This is a strong indication that the near-IR emitting regions (continuum and Br $\gamma$  line) have an approximately centrally-symmetric intensity distribution.

Since sgB[e] stars are thought to have non-spherical winds, we expect an elongated shape for their CSE projected onto the sky, unless the star is seen close to pole-on. Hereafter, we show that both AMBER and MIDI observations can indeed be well reproduced by an elliptical



Gaussian model for the CSE intensity distribution, corresponding to visibilities of the form:

$$V(u, v) = \exp \left\{ \frac{-\pi^2 (2a)^2}{4 \ln 2} [u^2 + (Dv)^2] \right\} \quad (1)$$

where  $u$  and  $v$  are the spatial-frequency coordinates,  $2a$  is the major-axis FWHM of the intensity distribution (image plane), and  $D$  is the ratio between the minor and major axes FWHM ( $D = 2b/2a$ ). Since, in general,  $2a$  forms an angle  $\alpha$  with the North direction (towards the East),  $u$  and  $v$  should be replaced in Eq. 1 by  $(u \sin \alpha + v \cos \alpha)$  and  $(u \cos \alpha - v \sin \alpha)$ , respectively. A preliminary analysis of  $V$  at each individual wavelength  $\lambda$  showed that  $D$  and  $\alpha$  can be considered independent on  $\lambda$  within a given spectral band ( $K$  or  $N$ ). On the other hand, the CSE size varies with  $\lambda$ , as seen from the  $\theta_{UD}$  curves in Figs. 2 and 3.

#### 4.1. Size and geometry in the $K$ band

We interpret the AMBER observations in terms of an elliptical Gaussian model (Eq. 1) with a chromatic variation of the size. The  $\theta_{UD}(\lambda)$  curves in Fig. 2 suggest a linear increase of the size within this part of the  $K$  band. In addition, the AMBER visibilities decrease significantly inside  $\text{Br}\gamma$ , indicating that the line-forming region is more extended than the region responsible for the underlying continuum. Based on these considerations, we adopted the following expression for the major-axis FWHM:

$$2a(\lambda) = 2a_0 + C_1(\lambda - \lambda_0) + C_2 \exp \left[ -4 \ln 2 \left( \frac{\lambda - \lambda_{\text{Br}\gamma}}{\Delta\lambda} \right)^2 \right] \quad (2)$$

where  $2a_0$  is the major-axis FWHM at a chosen reference wavelength  $\lambda_0 (= 2.2 \mu\text{m})$ , and  $C_1$  is the slope of  $2a(\lambda)$ . The size-increase within  $\text{Br}\gamma$  is modeled by a Gaussian with an amplitude  $C_2$  and FWHM  $\Delta\lambda$ , centered at  $\lambda_{\text{Br}\gamma} = 2.165 \mu\text{m}$ . Figure 2 shows a rather good fit of this model to the observed visibilities in both the continuum and inside  $\text{Br}\gamma$ . The parameters derived from the fit are listed in Table 4.

#### 4.2. Size and geometry in the $N$ band

Similar to the analysis of the AMBER visibilities, we interpret the MIDI observations of CPD-57° 2874 in terms of an elliptical Gaussian model (Eq. 1) with a size varying linearly with  $\lambda$  as given in Eq. 2 (for the analysis of the MIDI data the parameter  $C_2$  is set to zero). Additionally, since the  $\theta_{UD}$  curves show a stronger  $\lambda$ -dependence between 7.9 and 9.8  $\mu\text{m}$  compared to the region between 10.2 and 13.5  $\mu\text{m}$  (see Fig. 3), we performed an independent fit for each of these two spectral regions. The adopted elliptical Gaussian model also provides a good fit to the MIDI visibilities as shown in Fig. 3. The parameters corresponding to the fit in the two spectral regions within the  $N$  band are listed in Table 4.

To illustrate our results the model parameters given in Table 4 are visualized in Fig. 5.

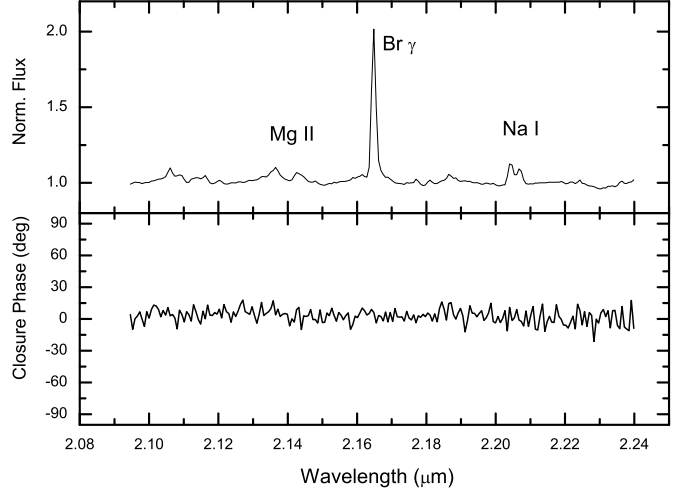


**Fig. 4.** VLTI/AMBER closure phase for CPD-57° 2874 obtained around  $\text{Br}\gamma$  with spectral resolution  $R = 1500$ . Within the noise level ( $\simeq \pm 10^\circ$ ) the closure phase is zero both in the continuum and in the  $\text{Br}\gamma$  line. This strongly suggests that the CSE has an approximately centrally-symmetric projected intensity distribution in the near-IR.

## 5. Discussion and conclusions

Our analysis of the VLTI spectro-interferometric data presented in Sect. 4 supports the hypothesis of a non-spherical CSE for sgB[e] stars.

In particular, the MIDI observations suggest that the hot-dust emission originates in an elongated structure (probably in an equatorial disk), which is in agreement with previous polarization measurements from Yudin & Evans (1998). After correction for the interstellar polarization, Yudin (private communication) estimated an intrinsic polarization position angle  $\simeq 45^\circ - 55^\circ$ . Interestingly, within the error bars this angle is perpendicular to the major-axis PA we derived from the MIDI data ( $\alpha \simeq 144^\circ$ ; see Table 4), as is expected from a disk-like dusty CSE. Under the disk hypothesis, the measured mid-IR flattening ( $D \simeq 0.76 - 0.80$ ; see Table 4) allows us to estimate an intermediate viewing angle for the non-spherical CSE ( $i \sim 30^\circ - 60^\circ$ ).

The contemporaneous recording of the AMBER and MIDI data enables us to compare the CSE structure in the near- and mid-IR. As shown in Table 4, the size, flattening, and orientation of the elliptical Gaussian model significantly changes from the  $K$  to the  $N$  band. For example, the region emitting the mid-IR flux ( $2a \geq 10 \text{ mas} = 25 \text{ AU}^2$  at  $\lambda \geq 8 \mu\text{m}$ ) is more than 2.5 times larger than the one emitting the near-IR continuum flux ( $2a \simeq 3.4 \text{ mas} = 8.5 \text{ AU}$  at  $\lambda \simeq 2.2 \mu\text{m}$ ).

If we correct the influence of the continuum on the visibility measured in  $\text{Br}\gamma$  (Malbet et al. 2005), we estimate the size (minor  $\times$  major axes) of the region responsible for the pure  $\text{Br}\gamma$  emission to be  $\simeq 2.8 \times 5.2 \text{ mas}$  (or  $\simeq 7.0 \times 13.0 \text{ AU}$ ). This size is  $\simeq 55\%$  larger than that of

<sup>2</sup> Adopting a distance  $d = 2.5 \text{ kpc}$ ; see Sect.3.

**Table 4.** Model parameters and  $\chi_{\text{red}}^2$  (reduced chi-squared) derived from the fit of an elliptical Gaussian (Eqs. 1 and 2) to the VLTI/AMBER and VLTI/MIDI visibilities. Angular sizes (in mas) correspond to FWHM diameters. The errors of the fit parameters include the calibration errors of the instrumental transfer function ( $\simeq 5\%$ ), estimated from all calibrator stars observed.

Instrument	$\lambda_0$ ( $\mu\text{m}$ )	major axis $2a_0$ (mas)	$C_1$ (mas/ $\mu\text{m}$ )	position angle $\alpha$	$D = 2b/2a$	minor axis $2b_0$ (mas)	Br $\gamma$ : $C_2$ (mas) <sup>a</sup>	Br $\gamma$ : $\Delta\lambda$ ( $10^{-3}\mu\text{m}$ )	$\chi_{\text{red}}^2$
AMBER	2.2	$3.4 \pm 0.2$	$1.99 \pm 0.24$	$173^\circ \pm 9^\circ$	$0.53 \pm 0.03$	$1.8 \pm 0.1$	$1.2 \pm 0.1$	$1.8 \pm 0.2$	0.7
MIDI (< 10 $\mu\text{m}$ )	8.0	$10.1 \pm 0.7$	$2.58 \pm 0.41$	$145^\circ \pm 6^\circ$	$0.76 \pm 0.11$	$7.7 \pm 1.0$			0.1
MIDI (> 10 $\mu\text{m}$ )	12.0	$15.3 \pm 0.7$	$0.45 \pm 0.22$	$143^\circ \pm 6^\circ$	$0.80 \pm 0.10$	$12.2 \pm 1.1$			0.1

<sup>a</sup> Corresponding to a FWHM major axis  $2a = 4.5 \pm 0.3$  mas and minor axis  $2b = D * 2a = 2.4 \pm 0.1$  mas at the center of the Br $\gamma$  line ( $\lambda_{\text{Br}\gamma} = 2.165 \mu\text{m}$ ).

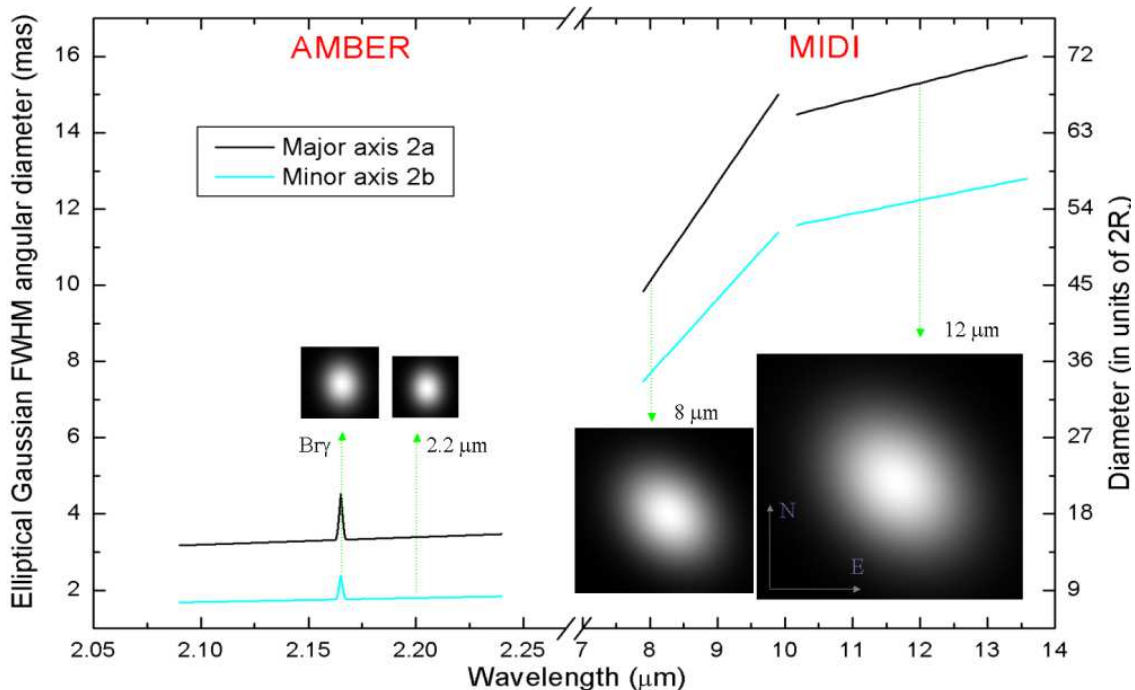


**Fig. 5.** This figure illustrates the results (size and orientation) derived from the fit of an elliptical Gaussian model (Eqs. 1 and 2) to the VLTI/AMBER and VLTI/MIDI visibilities (the corresponding fit parameters are listed in Table 4). The scale in the right is given in stellar diameters ( $2R_*$ ), where the radius  $R_*$  is estimated to be  $60 \pm 15 R_\odot$  (Sect. 3).

the underlying near-IR continuum, but more than 2 times smaller than the mid-IR emitting region ( $\lambda \geq 8 \mu\text{m}$ ). Near-IR diameters of  $\sim 10$  AU correspond to  $\sim 36R_*$  (assuming  $R_* = 60 R_\odot$ ; see Sect.3). This measurements are compatible the theoretical CSE diameters computed by Stee & Bittar (2001) for a classical Be star, though our data show a larger difference between the Br $\gamma$  and continuum sizes.

The differences in flattening and position angle of the elliptical models fitted to the AMBER and MIDI data are in agreement with the two-component CSE paradigm suggested for sgB[e] stars (Zickgraf et al. 1985). The mid-IR flux is probably solely due to dust emission from an equatorial disk. By contrast, the near-IR continuum flux distribution probably results from a complex interplay among the radiation from the central star, the tail of hot-dust

emission ( $T_{\text{dust}} \simeq 1500$  K), and the free-free and free-bound emission from the fast polar wind and the disk-wind interaction. The Br $\gamma$  emission does not necessarily follow the same geometry.

A detailed investigation of the CSE geometry in the near-IR (continuum and Br $\gamma$ ) requires additional interferometric observations covering a larger range of baselines and position angles. In addition, we believe that further MIDI observations at baselines longer than  $\simeq 80$  m should be performed to obtain higher spatial resolution of the innermost parts of the dusty CSE. This would allow one to investigate more deeply how close to the hot central star ( $T_{\text{eff}} \simeq 20000$  K) the dust is formed.

Moreover, the combination of interferometric resolution, multi-spectral wavelength coverage and relatively

high spectral resolution now available from the VLTI, requires the development of interferometry-oriented and physically-consistent models for sgB[e] stars. We hope that the present work will motivate the development of such models, as well as open the door for new spectro-interferometric observations of these complex and intriguing objects.

## 6. Acknowledgments

A.D.S. acknowledges the Max-Planck-Institut für Radioastronomie for a postdoctoral fellowship. We thank the JMMC-France user-support for information about the ASPRO software. We are indebted to Dr. R. V. Yudin for his calculations on the intrinsic polarization vector.

## References

- Carlson, E. D., & Henize, K. G. 1979, *Vistas in Astronomy*, 23, 213
- Carter, B. C. 1990, *MNRAS*, 242, 1
- Cutri, R. M., Scrutskie, M. F., Van Dyk, S., et al. 2003, *The 2MASS All-Sky Catalog of Point Sources*, University of Massachusetts and Infrared Processing and Analysis Center (IPAC/California Institute of Technology)
- Drilling, J. S. 1991, *ApJS*, 76, 1033
- Herbig, G. H. 1993, *ApJ*, 407, 142
- Humphreys, R. M. & Davidson, K. 1979, *ApJ*, 232, 409
- Jaffe, W. 2004, *Proc. SPIE*, 5491, 715
- Kraus, M., & Lamers, H. J. G. L. M. 2003, *A&A*, 405, 165
- Lamers, H. J. G. L. M., & Pauldrach, A. W. A. 1991, *A&A*, 244, L5
- Lamers, H. J. G. L. M., Zickgraf, F., de Winter, D., Houziaux, L., & Zorec, J. 1998, *A&A*, 340, 117
- Leinert, Ch., van Boekel, R., Waters, L.B.F.M., et al. 2004, *A&A*, 423, 537
- Magalhães, A. M. 1992, *ApJ*, 398, 286
- Malbet, F., Benisty, M., de Wit, W. J., et al. 2005, *A&A*, submitted
- McGregor, P. J., Hyland, A. R., & Hillier, D. J. 1988, *ApJ*, 324, 1071
- Menzies, J. W., Marang, F., Laing, J. D., Coulson, I. M., & Engelbrecht, C. A. 1991, *MNRAS*, 248, 642
- Millour, F., Tatulli, E., Chelli, A. et al. 2004, *Proc. SPIE*, 5491, 1222
- Petrov, R. G., Malbet, F., Weigelt, G., et al. 2003, *Proc. SPIE*, 4838, 924
- Richichi, A., Percheron, I., & Khristoforova, M. 2005, *A&A*, 431, 773
- Sloan, G. C., Kraemer, K. E., Price, S. D., & Shipman, R. F. 2003, *ApJS*, 147, 379
- Stee, P., & Bittar, J. 2001, *A&A*, 367, 532
- Swings, J.-P., & Allen, D. A. 1972, *PASP*, 84, 523
- Wackerling, L. R. 1970, *Mem. RAS*, 73, 153
- Yudin, R. V., & Evans, A. 1998, *A&AS*, 131, 401
- Zickgraf, F.-J. 2003, *A&A*, 408, 257
- Zickgraf, F.-J., Wolf, B., Stahl, O., Leitherer, C., & Klare, G. 1985, *A&A*, 143, 421